Clays and Clay Minerals, Vol. 45, No. 3, 448–460, 1997.

SURFACE STRUCTURAL MODEL FOR FERRIHYDRITE

A. MANCEAU AND W. P. GATES†

Environmental Geochemistry Group, LGIT-IRIGM, University Joseph Fourier and CNRS, 38041 Grenoble Cedex 9, France

Abstract—A structural model for the geometry of Fe(III) octahedra near the surface of finely divided ferrihydrite was elaborated based on the bond–valence theory and by considering the interaction of water molecules in the 2 nearest hydration spheres. In contrast to bulk Fe atoms, which are bonded to bridging oxo (O) and hydroxo (OH) ligands, surface Fe atoms are also octahedrally coordinated to H_2O ligands forming the 1st hydration shell ($(H_2O)_I$). In the wet state, external water molecules of the 2nd hydration shell ($(H_2O)_{II}$) are singly H-bonded to $(H_2O)_I$, while they are doubly coordinated in the dry state. Accordingly, wet ferrihydrite contains twice as many sorbed water molecules as dry ferrihydrite, and the structural difference due to the 2nd hydration shell accounts quantatively for the 15% increase of ferrihydrite weight experimentally measured in moist atmosphere. The interaction of surface Fe atoms with their 2 nearest hydration spheres modifies the geometry of surface Fe octahedra as compared to bulk octahedra, and idealized Fe-OH and Fe-H_2O bond lengths in the wet and dry state were evaluated by the bond–valence theory. Our structural model provides a sound crystal–chemical basis to describe many apparent incongruities of Fe X-ray absorption near edge structure (*K*-XANES) and extended X-ray absorption fine structure (EXAFS) spectroscopic data that have led to differing interpretations of the coordination environment of Fe in ferrihydrite by various investigators.

Key Words—EXAFS, Ferrihydrite, Hydrous Ferric Oxide, XANES, X-ray Absorption Spectroscopy.

INTRODUCTION

Since Chukhrov et al. (1973) first identified ferrihydrite (Fh), many studies have been conducted to determine its structural details. Independent studies have resulted in contrasting interpretations of the coordination of ferric iron in Fh by XANES spectroscopy. The octahedral coordination of Fe atoms in the ferrihydrite structure was initially determined by Fe *K*-edge XANES spectroscopy (Manceau et al. 1990) and confirmed by EXAFS spectroscopy (Manceau and Drits 1993). On the basis of spectral shape and intensity analysis, Manceau et al. (1990) concluded that 4-fold Fe was absent within detection limits (10%). Zhao et al. (1994), using XANES, suggested that 20 to 30% of surface Fe atoms in ferrihydrite powder are coordination-unsaturated, presumably in a 4-fold coordination. A comprehensive structural model for 2-line and 6-line Fh, which accounts for X-ray diffraction (XRD), EXAFS (Manceau and Drits 1993) and XANES (Manceau et al. 1990) measurements, has been recently proposed by Drits et al. (1993). According to this model, ferrihydrite is a mixture of 3 components: 1) defect-free Fh consisting of anionic ABACA . . . close packing in which Fe atoms occupy only octahedral sites with 50% probability (space group $P\bar{3}1c$); 2) defective Fh in which Ac_1Bc_2A and Ab_1Cb_2A structural fragments occur with equal probability and alternate completely at random; and 3) ultradispersed hematite grains with mean dimension of coherent scattering domains of 10–20 Å.

Hydrous ferric oxides, and specifically ferrihydrite, are common constituents of subsurface environments. Their high surface reactivities are believed to influence many geochemical reactions, such as the sorption and retention of soil contaminants (Manceau et al. 1992; Manceau and Charlet 1994; Spadini et al. 1994; Manceau 1995) and plant nutrients (Parfitt et al. 1975). Fundamental knowledge of surface structural properties (that is, coordination and geometry of the Fe atoms at or near the surface) of poorly crystalline phases of Fe is thus a prerequisite for determining the sorption mechanism of sorbates at the molecular level, and for understanding ferrihydrite metastability and its transformation to more crystalline phases.

The goals of this paper are 2-fold. The 1st is to bring attention to instrumental and operator sources of error that are root causes of diverging interpretations of the coordination of Fe in ferrihydrite, and describe experimentally how this relates to the crystal chemical information obtained. The 2nd goal is to propose a simple, geometric model for the structure of surface Fe octahedra in ferrihydrite that builds on the earlier model of Drits et al. (1993), and to show how this model can explain several of the inconsistencies in the quantitative interpretation of XANES and EXAFS spectra by Zhao et al. (1993, 1994).

BACKGROUND

During X-ray excitation in a *K*-edge XANES experiment, an electron from an inner shell of an atom is ejected with increasing kinetic energies to: 1) tightly bound (stabilized) unfilled molecular orbital (MO) levels; 2) weakly bound (destabilized) unfilled MO levels; and 3) the continuum, or the surrounding "molecular"

† Present address: Savannah River Ecology Laboratory, The University of Georgia, Drawer E, Aiken, South Carolina 29802.

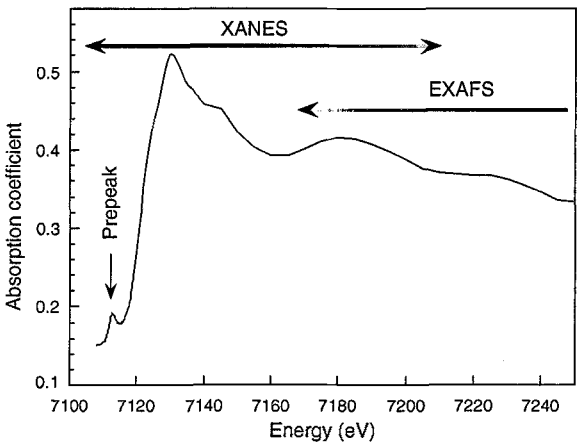

Figure 1. XANES and EXAFS regions in X-ray absorption spectra.

cage (Bianconi 1988). For the sake of convenience, 2 distinct regions of a XANES spectrum will be considered: the low-energy "pre-edge" region immediately prior to the main absorption edge threshold, and the high-energy region, which includes the main absorption edge and extends approximately 100 eV beyond (Figure 1). The intensity of absorption features is predominantly ruled by dipolar selection rules. Excitation of a core state electron with an orbital angular momentum l probes the $l + 1$ and $l - 1$ unfilled MO levels. Accordingly, absorption K-edge features reflect the unoccupied density of states of p-like character and the main absorption discontinuity results from $1s \rightarrow np$ transitions ($n = 4$ for Fe K-edge). The weak pre-edge structure (prepeak) observed at the bottom of the steeply rising Fe K-edge discontinuity of transition metal complexes corresponds to $1s \rightarrow 3d$ transitions (Calas and Petiau 1983).

Coordination of ligands causes the splitting of degenerate $3d$ orbitals to $e_g + t_{2g}$ MO levels for O_h and $t_2 + e$ for T_d symmetry. Point group selection rules for dipolar transitions indicate that $3d$ transitions are not allowed in O_h symmetry, whereas in T_d symmetry the $1s(a_1) \rightarrow t_2$ transition is allowed. If a distortion is introduced at the site of the cation, such as trigonal (C_{3v}) distortion in O_h, a portion of the formerly forbidden transitions becomes allowed. These geometrical considerations only determine whether a transition is forbidden as long as the electronic distribution has the same symmetry as the atomic site, which is the case only for pure atomic states. In solids, the charge distribution is of lower symmetry than the point symmetry of the site due to hybridization of metal d-orbitals with ligand p-orbitals ($\Delta l = 1$). Ultimately, the prepeak intensity depends on both local symmetry as well as electronic properties of the cation and is actually very low for common octahedral sites, whereas tetrahedral arrangements give rise to rather high amplitudes.

Comparison of the normalized Fe K pre-edge spectra of various references in Figures 2a and 2b (Combes et al. 1989; Manceau et al. 1990) leads to the following observations. First, prepeaks increase in energy due to an increase in binding energy of the $1s$ electron and the destabilization of antibonding states as the formal valency of the metal ion increases (Table 1). Second, the prepeaks of 6-fold coordinated Fe are split into t_{2g}- and e_g-like components with a separation of $\approx$1 eV, whereas in a tetrahedral coordination (such as $FePO_4$) the e- and t_2-like levels are close in energy (Douglas et al. 1994), and therefore appear as a single peak. An example of this is magnetite, where ⅓ of the Fe is tetrahedrally coordinated (Table 1). Third, the prepeak intensity for ^{VI}Fe(II) is lower than ^{VI}Fe(III) because the oscillator strength of the transition logically increases with the emptiness of the $3d$ level [Fe(II) has a $3d^6$ and Fe(III) a $3d^5$ electronic structure], and also because metal $3d$ and oxygen $2p$ mixing are greater for trivalent than for divalent Fe (Sherman 1985).

Spectral features of the main absorption edge region are due to transitions to continuum states and reflect resonance or multiple scattering (MS) processes of the excited electron within a "molecular" cage around the metal (Bianconi 1988). From the viewpoint of electron path, 2 different regions may be distinguished within this portion of a XANES spectrum. Single and multiple scattering processes involving O atoms from the 1st coordination shell produce the main contribution to structures observed below and just above the edge crest. The energy range extending past the edge crest to $\approx$100 eV is characteristic of the extended local structure ($\approx$3 neighboring shells) of the absorbing atom. Thus, main-edge features are sensitive to the short- and medium-range order around the metal site. Therefore, as one might expect, similar crystalline structures result in similar spectra, both in the position and amplitude of features. Distinction between localized and extended scattering events are supported by recent *ab initio* MS calculations performed on FeO_4, FeO_6 and $FeO_{12}Si_8Mg_6O_{22}$ clusters (Farges 1995). XANES spectra for isolated FeO_4 and FeO_6 clusters differed by their position and shape in the vicinity of the edge crest. Specifically, tetrahedral coordination leads to a marked shoulder in the steeply rising absorption edge itself and a shift of the edge maximum to higher energy. This effect has been experimentally observed by many authors on a number of inorganic compounds, and is often used as a fingerprint for tetrahedral configuration (Waychunas et al. 1983; Waychunas et al. 1988; Combes et al. 1989). We have illustrated this in Figure 3a for $FePO_4$ and Fe oxyhydroxides.

https://doi.org/10.1346/CCMN.1997.0450314 Published online by Cambridge University Press

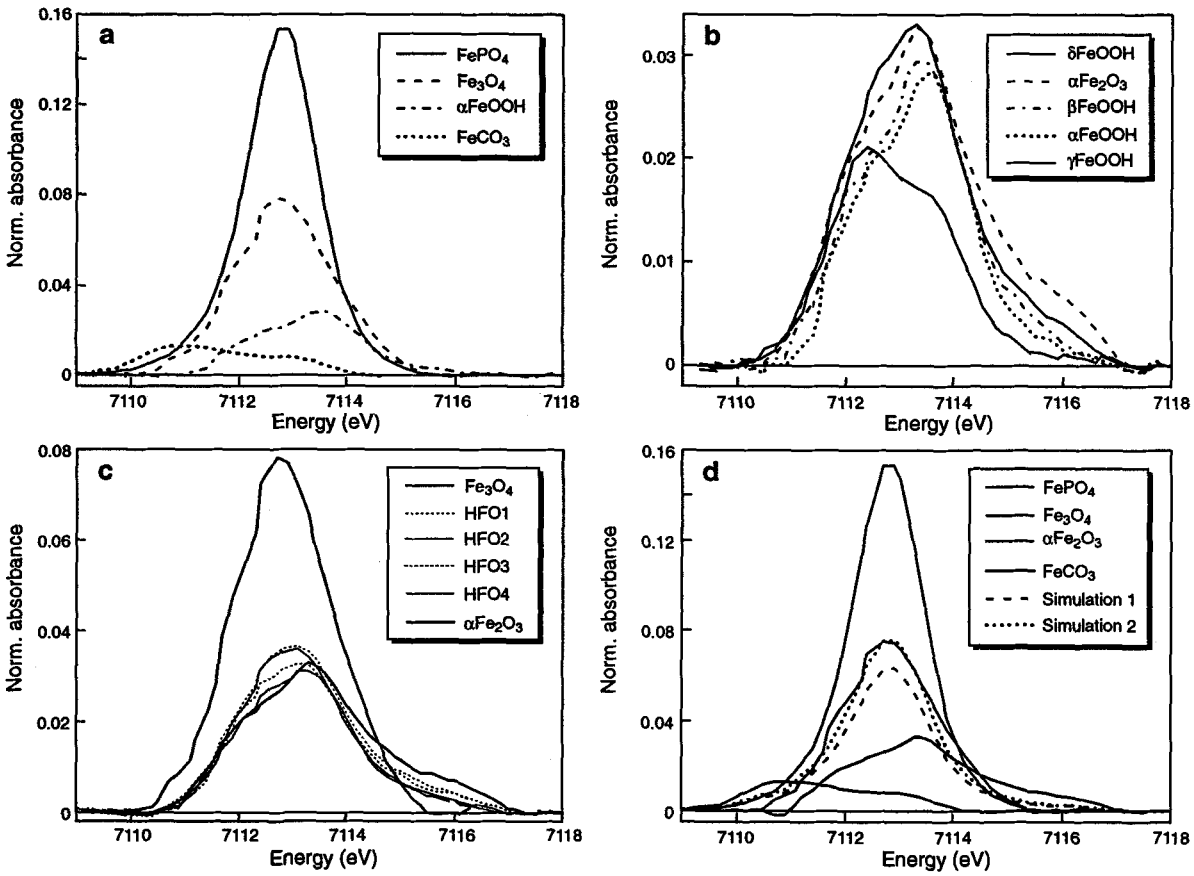

Figure 2. Normalized Fe *K*-edge prepeak spectra for reference compounds and hydrous ferric oxide samples. In a), b) and c) sample names are ranked in the order of decreasing pre-peak amplitude.

An elegant demonstration of the localized character of scattering resonances observed below the edge crest comes from a recent polarized XANES study on epidote (Henderson et al. 1995). The relative intensities of spectral features below the edge crest were shown to depend on the orientation of the Fe-O bond relative to the electric field vector, thus demonstrating that MS path resonances were occurring in the cage delimited by the ligand sphere. Proper modeling of the detailed spectral features observed in the extended region requires consideration of larger scattering paths extending beyond the first ligand shell, the length of which critically depends on the insulating vs. conducting character of the solid. For enstatite, Farges (1995) showed that high-energy XANES features were accurately reproduced by extending MS calculations up to 4.5 Å in an $FeO_{12}Si_8Mg_6O_{22}$ cluster.

Table 1. Selected mineralogical and crystallographic information about reference minerals.

Mineral name	Structural formula	Oxidation state and site occupation of cation
Goethite	α FeOOH	^{VI}Fe(III)
Akaganeite	β FeOOH	^{VI}Fe(III)
Lepidocrocite	γ FeOOH	^{VI}Fe(III)
Feroxyhite	δ FeOOH	^{VI}Fe(III)
Hematite	α Fe_2O_3	^{VI}Fe(III)
Iron phosphate	$FePO_4$	^{IV}Fe(III)
Siderite	$FeCO_3$	^{VI}Fe(II)
Maghemite	γ Fe_2O_3	^{IV}Fe(III) + ^{VI}Fe(III)
Magnetite	Fe_3O_4	^{IV}Fe(III) + ^{VI}Fe(III) + ^{VI}Fe(II)

EXPERIMENTAL

Four hydrous ferric oxide samples were examined: HFO1, HFO2, HFO3 and HFO4. The first 3 are 2-line ferrihydrites obtained by the complete hydrolysis of solutions of ferric nitrate (HFO1), ferric chloride (HFO2) and ferric perchlorate (HFO3). HFO4 is a 6-line ferrihydrite. Details of their preparation are found elsewhere (Combes et al. 1989; Combes et al. 1990; Spadini et al. 1994). XANES spectra were recorded in transmission mode on the EXAFS I station at the Labratoire pour l'Utilisation du Rayonnement Electromagnétique (LURE) synchrotron radiation facility (Orsay, France). The electron energy of the DCI storage ring was 1.85 GeV and the current was between 250 and 300 mA. This 1st generation synchro-

https://doi.org/10.1346/CCMN.1997.0450314 Published online by Cambridge University Press

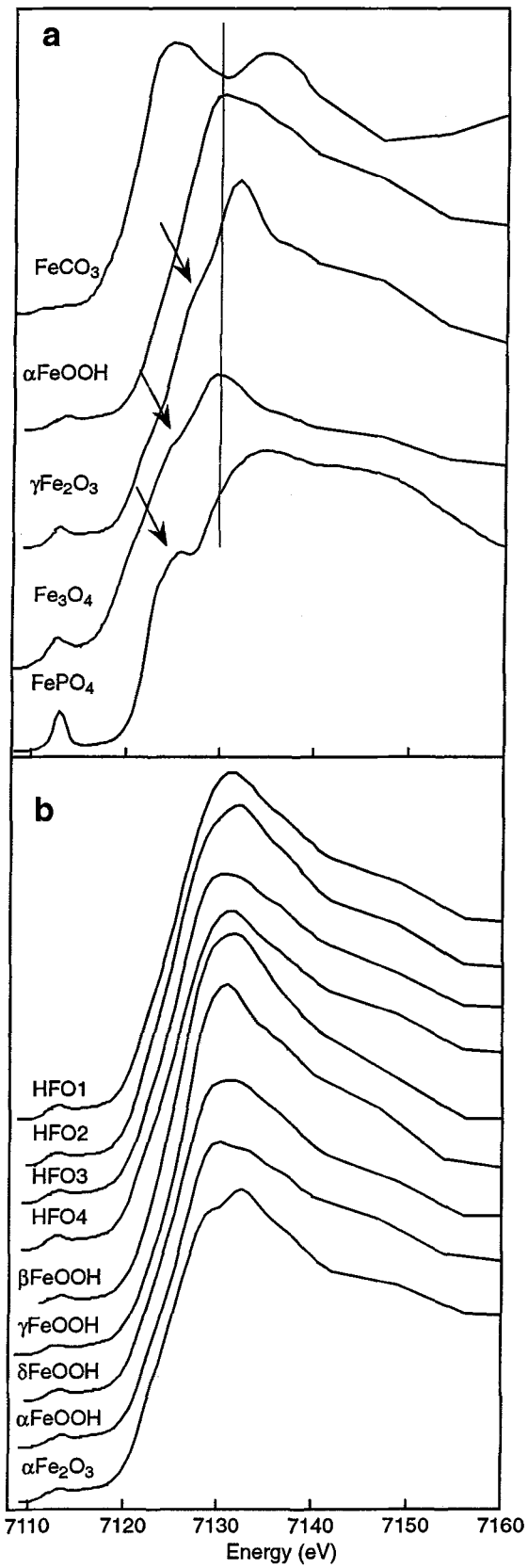

tron source delivers the incident beam with a degree of divergence as high as 10^{-4} radian and, consequently, an Si(331) channel-cut crystal was used to improve the spectral resolution. Under these conditions the energy resolution was ≈1.5 eV, which is slightly less than the Fe core level width of 1.1 to 1.2 eV (Parratt 1959; Muller et al. 1982). For the sake of consistency, the same energy calibration as in the work of Manceau et al. (1990) was chosen. Prepeak spectra were processed by subtracting a least-squares fit of a 2nd-order polynomial to the absorption background 3 eV from both sides of the pre-edge peak. The absorbance was then normalized to the absorption jump of the main edge ($\Delta\mu$), determined by fitting a 1st-order polynomial to the data 500 eV above the edge. Previously we fit the absorption background with an arctangent function instead of a polynomial function as in the present study. This new normalization procedure resulted in a decrease of the prepeak height as compared to former studies, but is without effect on the interpretation of data since we are concerned with *relative* variation of intensities. The new procedure resulted in a normalized intensity of 0.08 for magnetite (Figure 2a), which is precisely the value reported recently by Bajt et al. (1994) for the same mineral.

RESULTS AND DISCUSSION

Pre-edge Spectra

Comparison of the prepeak spectra for ferrihydrite samples and a selection of Fe oxide references (Figure 2c, Table 1) clearly indicates that Fe atoms in ferrihydrite are predominantly 6-fold coordinated. The presence of ^{IV}Fe was inferred by Zhao et al. (1994) on the basis of pre-edge intensity and shape. Indeed, the prepeaks for ferrihydrite samples display a single maximum (as for magnetite) of slightly higher intensity than those for goethite and hematite. However, their interpretation is questionable, since the amount of tetrahedrally coordinated Fe was estimated from prepeak intensity using magnetite (^{IV}Fe(III) ^{VI}Fe(III) ^{VI}Fe(II)O_4) as a reference for ^{IV}Fe(III) species and assuming: 1) a peak area ratio of 1:2:3 for 6, 5 and 4 coordination, respectively (Roe et al. 1984); and 2) an oscillator strength of ⅓ × 3 = 1.0 for the ^{IV}Fe(III) component and ⅔ × 1 = 0.67 for the 2 octahedral magnetite components. These assumptions predict an intensity of 1.67 for magnetite compared to 1.00 for goethite and hematite. The agreement of the calculated and experimental intensities was apparently verified (Zhao et al. 1994), since the peak intensities were found to be equal to 0.074 and 0.077 for hematite and goethite, and 0.141 for magnetite. However, it will be shown

←

Figure 3. Normalized Fe *K*-edge XANES spectra for reference compounds and hydrous ferric oxide samples.

https://doi.org/10.1346/CCMN.1997.0450314 Published online by Cambridge University Press

below that this agreement is completely fortuitous and is related to 2 compensating errors.

First, the estimation of the oscillator strength for 6-coordinate Fe in magnetite is misleading, since it is based on the implicit inference that ^{VI}Fe(III) and ^{VI}Fe(II) species have the same oscillator strength. As indicated above, spectra of reference compounds (Figure 2a) indicate that the prepeak intensity for divalent Fe ($FeCO_3$) is about half that of trivalent Fe (FeOOH) due to differences in electron density in the 3*d* level. Therefore, the assumption that Fe(II) and Fe(III) have identical oscillator strengths is in error. A new estimation of the contribution of 6-coordinate iron is: ⅓ × 1 (^{VI}Fe(III) species) + ⅓ × ½ (^{VI}Fe(II) species) = 0.50, leading to a magnitude for the whole magnetite prepeak of ≈0.075 × 1.5 = 0.112, notably lower than the experimental one (0.141).

The underestimation of the new prepeak intensity comes from a 2nd source of error, that is, the ratio of oscillator strengths between ^{VI}Fe(III) and ^{IV}Fe(III) species. Zhao et al. (1994) used a ratio of 1:3 determined from the analysis of a series of ferric coordination complexes (Roe et al. 1984). Perusal of Roe's work reveals that this ratio ranged from 1:2.3 to 1:5 for different model compounds. Variation in this ratio is not surprising since the electronic structure of Fe 3*d* orbitals in coordination complexes is known to strongly vary with the nature of the ligand (Douglas et al. 1994). A ratio of 1:4 to 1:5 was estimated by Combes et al. (1989) and Manceau et al. (1990) using $FePO_4$ as a reference for ^{IV}Fe(III) (Figure 2). Based on this ratio, the new theoretical prepeak magnitude for magnetite is [⅓ × 4(^{IV}Fe(III) species) + 0.5 (^{VI}Fe species)] × 0.075 = 0.137, a value now very close to the experimentally determined 0.141. Thus, failure to properly consider the different oscillator strengths of the various Fe species in magnetite contributed to a mistaken estimation of the percentage of lower-coordinate ferric iron in ferrihydrite samples. These results point to the importance of using model compounds with similar electronic properties and crystalline structures as the unknown sample in order to properly attribute spectral properties to various coordination environments.

The absence of well-resolved splitting of the prepeak spectra for Fh was interpreted by Zhao et al. (1994) as additional evidence for the presence of ^{IV}Fe(III). However, prepeak shape is also sensitive to variations in the local symmetry of the Fe site. Figure 2b shows that the shape of the prepeak for lepidocrocite is unique, with $I(t_{2g}) > I(e_g)$, whereas the reverse situation is observed in other ^{VI}Fe(III) references. According to the Fh structural model of Drits et al. (1993), Fe atoms have many different local environments, which can be viewed as α,β,γFeOOH-like and αFe_2O_3-like local domains. Their model fully accounts for the variety of structural environments surrounding Fe atoms as determined by Mössbauer spectroscopy (Cardile 1988) and provides a reasonable explanation for the relative broadening of Fh pre-edge spectra as compared to pure crystalline references where the Fe site is unique.

Thus, it follows that a stringent evaluation of the validity for using magnetite as an ^{IV}Fe(III) reference in determining Fe occupancy of unknown compounds consists simply of comparing its prepeak intensity with pure ^{VI}Fe(III) and ^{IV}Fe(III) references. If the method was fully self-consistent with respect to the evaluation of the site occupancy of Fe in minerals, the Fe_3O_4 spectrum should be reproduced by a linear combination of reference spectra for ^{VI}Fe(III), ^{IV}Fe(III) and ^{VI}Fe(II) species. Figure 2d contrasts the experimental magnetite spectrum with those obtained computationally using the following weighted schemes: simulation 1 = ⅓ $FeCO_3$ + ⅓ αFeOOH + ⅓ $FePO_4$, and simulation 2 = 1.2 × simulation 1. Simulation 1 is 20% less intense than the experimental spectrum (Figure 2d), illustrating the limitations of pre-edge spectroscopy in evaluation of cation site occupancy in minerals.

Prepeak Intensity Enhancement in Ferrihydrite

Ferrihydrite samples do have a prepeak intensity that sometimes is substantially greater than ^{VI}Fe(III) references (Figure 2c). Our results indicate that the increase in intensity of Fh pre-edge spectra for dry samples as compared to hematite ranges between 0 and 20% (Figure 2c). The range reported by Zhao et al. (1994) is much greater, from 20 to 80%. This large intensity variation was interpreted as a reduction from 6- to 4-fold coordination of surface Fe atoms in going from the wet to dry state, that is, as the result of dehydroxylation. Although the presence of a few percent tetrahedral Fe (or even 5-fold coordinated Fe) cannot be completely discarded based on results currently available, the finding that up to 20–30% ^{IV}Fe(III) exists (Zhao et al. 1993; Zhao et al. 1994) is questionable because the prepeak intensity is not uniquely related to the coordination number of cations in solids, but also to the geometry of the Fe sites (compare background section). In addition, it will be shown later on that this coordination change conflicts with both main-edge and EXAFS results. In the following section, 2 alternative explanations of ferrihydrite prepeak enhancements will be successively examined.

GEOMETRY OF SURFACE FE SITES. In finely dispersed ferrihydrite grains, up to 35% Fe may be located at the surface (Zhao et al. 1993) and Fe atoms can be coordinated to O, OH and H_2O ligands (Russell 1979; Stanjek and Weidler 1992; Drits et al. 1993). Based on simple valence charge balance considerations, one will find that oxygens are linked to several Fe atoms, whereas H_2O can only be bonded to a single Fe atom.

As a consequence, bulk and surface Fe atoms are not equivalent, the former being predominantly bonded to O and OH ligands (oxo- and hydroxo-bridges) and the latter to H_2O and OH ligands.

Differences of bond lengths between bulk and surface Fe atoms can be estimated by using a simple bond–valence description of solids developed by Brown and coauthors (Brown and Shannon 1973; Brown 1981; Brown 1992), which is based on the concept of bond strength first introduced by Pauling (1929). The bond strength of a cation–anion pair (ij) is given by the ratio v_{ij} = cation charge/cation coordination, that is, for any ^{VI}Fe(III)-O pair, $v_{ij} = 3/6 = 0.5$ v.u. (valence unit). Pauling's electroneutrality principle states that the sum, Σv_{ij}, over all bonds formed by an ion, is equal to the formal valence of this ion, V_i, that is:

$$V_i = \sum_j v_{ij} \quad [1]$$

Due to disruption of the lattice near the surface, surface oxygens are undersaturated and charge neutralization is achieved by protons, resulting in the presence of -OH and/or -OH_2 surface groups. Distances of Fe-(O, OH, H_2O) bonds can be predicted by using indifferently either one of the 2 classical bond valence–bond length relationships (Brown 1981, 1992):

$$v_{ij} = (D1_{ij}/R_{ij})^N \quad [2]$$

$$v_{ij} = \exp[(D2_{ij} - R_{ij})/B] \quad [3]$$

where R_{ij} is the length of the bond between atoms i and j, and $D1$, $D2$, B and N are constants associated with the bonding pair that were determined empirically from a systematic analyses of several thousands of inorganic structures (Brown and Shannon 1973; Brown and Altermatt 1985; Brese and O'Keefe 1991). For instance, $D1_{Fe^{III}\text{-}O} = 1.78$; $N_{Fe^{III}\text{-}O} = 5.70$ (Brown 1981); $D2_{Fe^{III}\text{-}O} = 1.76$; $B = 0.37$ (Brown and Altermatt 1985). Fe-O and Fe-OH bond valences in αFeOOH were calculated by using these constants and the bond lengths determined by Szytula et al. (1968). Note in Figure 4 that the valence sum of Fe in bulk octahedra is equal to its formal charge (+3).

In light of the above considerations, a simple geometrical model for the hydration of surface Fe(III) ions in ferrihydrite can be constructed. Metal ions, whether at the surface of a solid or in solution, interact with a 2nd shell of water molecules, $(H_2O)_{II}$, and electroneutrality is realized through coordination with this 2nd hydration sphere (Figure 4). Surface $(H_2O)_I$ and $(OH)_I$ ligands are directly coordinated to Fe, and the external $(H_2O)_{II}$ water molecules are held to these ligands by O_I-H···O_{II} bonds (H-bonds) of variable strength. The $(H_2O)_{II}$ molecules interact either with a single O_I-H group ($(H_2O)_{II}^{strong}$), resulting in an O_I-H···O_{II} H-bond angle of about 180° (trigonal orientation), or are H-bonded simultaneously to 2 different surface O_I-H groups ($(H_2O)_{II}^{weak}$) and make a smaller O_I-H···O_{II} angle (pyramidal orientation) (Figure 4). A normal H-bond valence of 0.17 v.u. for $(H_2O,OH)_I$-$(H_2O)_{II}^{weak}$ H-bond interaction corresponds to a O_I-H···O_{II} angle of 165°, but can be as low as 130° for loosely bound water molecules (Brown 1976). Due to the lower coordination of the oxygen in $(H_2O)_{II}^{strong}$, the H-bond valences are stronger (that is, 0.25 v.u., Caminiti et al. 1978) (Figure 4). The $(H_2O)_I$-$(H_2O)_{II}^{strong}$ configurations are found in-6-coordinate trivalent metal aqua species ($Me(H_2O)_6^{3+}$) where the Me-O bond valence of 0.5 (3/6) is too strong to be fully balanced by the $(H_2O)_I$ shell (Brown 1976, 1981).

By analogy with solvated chromium (Caminiti et al. 1978), adsorbed $H_2O_{II}^{strong}$ molecules can be viewed as reminiscent of the structure of hexa-aqua $Fe(H_2O)_6^{3+}$ complexes. The presence of $(H_2O)_{II}^{strong}$ molecules on wet surfaces is also supported by energetic considerations. Since the sum of H-bond valences of $(H_2O)_{II}^{weak}$ molecules is greater than that of $(H_2O)_{II}^{strong}$ molecules ($0.17 \times 2 = 0.34$ vs. 0.25, Figure 4), $(H_2O)_{II}^{strong}$ molecules are comparatively weakly held to the mineral surface. In other words, since $(H_2O)_{II}^{strong}$ molecules are singly, and $(H_2O)_{II}^{weak}$ molecules doubly, coordinated to the mineral surface, the former configuration is less stable. Accordingly, since $(H_2O)_{II}^{strong}$ species are more stable in aqueous medium and are comparatively loosely bound to mineral surface, it seems reasonable to assume that their proportion ought to increase with sample humidity and decrease upon dehydration.

If we consider that a wet surface is covered only by $(H_2O)_{II}^{strong}$ and a dry surface by $(H_2O)_{II}^{weak}$ molecules then, for geometrical reasons, one must admit that in the wet state, ferrihydrite would contain twice as much physisorbed (H-bonded) $(H_2O)_{II}$ water as in the dry state. The increased mass caused by the addition of $(H_2O)_{II}^{strong}$, and the resulting change in the structure of the solvation shell upon wetting can be estimated from the chemical formula of $5Fe_2O_3 \cdot 9(H_2O)_I$ for ferrihydrite and assuming an $(H_2O)_{II}/(H_2O)_I$ ratio of 1 in the dry and 2 in the wet state. The increase of ferrihydrite weight in moist atmosphere predicted by our structural model is 14%. This value is in good agreement with the experimental one of 15% reported by Zhao et al. (1994).

The formation of H-bonds between $(H_2O)_I$ and $(OH)_I$ Fe ligands and external 2nd shell $(H_2O)_{II}$ molecules, readily influence Fe-O bond valences and, in turn, modify Fe-O bond lengths of surface vs. bulk Fe octahedra. The Fe-$(H_2O)_I$ distances calculated with the above-cited bond valence–bond length relationships are equal to 2.01 and 2.15 Å, and Fe-$(OH)_I$ distances to 1.93 and 1.96 Å (Figure 4). Of course, distances estimated by the bond strength–bond length theory should be considered as extreme values for the 2 octahedral Fe sites, and a range of intermediate distances probably exists in the ferrihydrite surface. Neverthe-

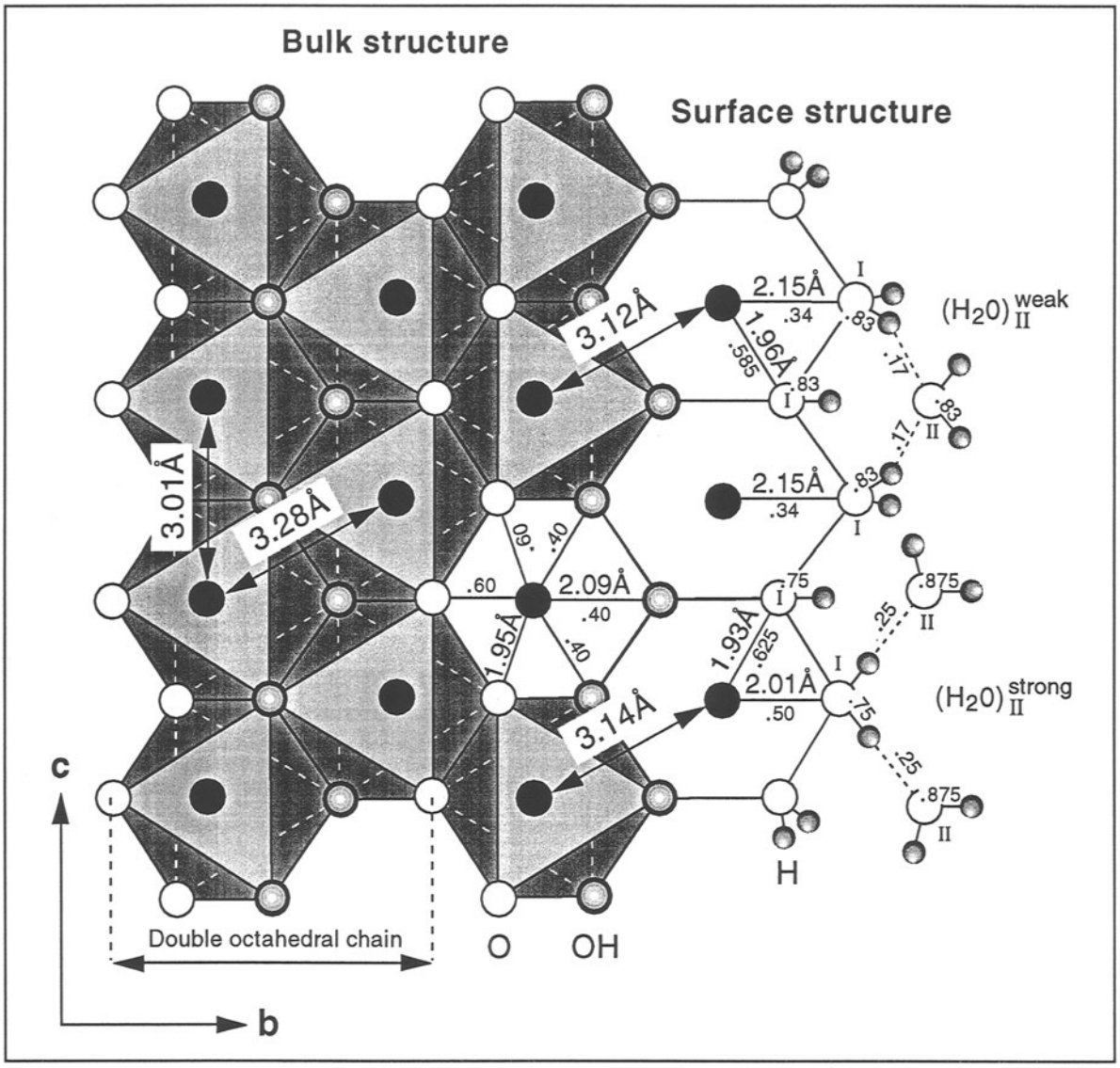

Figure 4. Structural model for the structure of surface Fe octahedra in ferrihydrite. The bulk structure of ferrihydrite is modeled after that of goethite (Drits et al. 1993; Spadini et al. 1994). Two double octahedral chains of goethite are projected in the *bc* plane. Small fractions indicate bond valence values for Fe-O and O-H and H···O bonds.

less, a direct consequence of this model is to show that bulk and surface Fe octahedra have a different distribution of bond lengths and, consequently, a different geometry. Owing to the large proportion of surface Fe atoms in ferrihydrite, this difference in site geometry is believed to account for most of the additional prepeak enhancement of dry ferrihydrite powders as compared to well-crystallized references.

Zhao et al. (1994) instead assumed that the relatively strong enhancement of ferrihydrite prepeak intensity upon drying resulted from a coordination change of surface Fe atoms, that is, to formation of coordination unsaturated (CUS) surface sites. But $(H_2O)_I$ molecules correspond to crystallization water and, owing to the overall strength of the Fe-$(H_2O)_I$ bond, removal requires significant inputs of energy. Typically, dehydroxylation of crystallization water (and subsequent loss of coordination) requires temperatures above 300–400 °C. In chalcophanite, a Zn-containing phyllomanganate, zinc octahedra lie above and below lattice vacancies and its coordination polyhedron consists of 3 oxygens linked to underlying Mn atoms and 3 $(H_2O)_I$ molecules directed towards the interlayer space (Wadsley 1955; Post and Appleman 1988). The removal of these structural water molecules is achieved at ≈300 °C (Dasgupta 1974).

The present structural model also offers a credible alternative explanation for the enhanced prepeak intensity

https://doi.org/10.1346/CCMN.1997.0450314 Published online by Cambridge University Press

of ferrihydrite samples upon air drying. The calculated Fe-$(H_2O)_I$ bond valence is lower when $(H_2O)_I$ molecules are H-bonded to $(H_2O)_{II}^{weak}$ molecules than to $(H_2O)_{II}^{strong}$ molecules (0.34 vs. 0.50, Figure 4). Consequently, the amount of long-distance Fe-$(H_2O)_I$ bonds in surface Fe octahedra is much larger in the dry than in the wet state. Stated another way, in the wet state, Fe-$(H_2O)_I$ distances are relatively short (for example, ≈2.01 Å), whereas in the dry state they are much larger (for example, ≈2.15 Å). Accordingly, enhancement of the prepeak intensity may be simply due to increasing distortion of surface Fe octahedra caused by the departure of loosely bound water in the external shell.

The structural interpretation by Zhao et al. (1993, 1994) is also doubtful for steric reasons. Based on Fe-O bond distance calculation ($<d(^{VI}Fe^{III}\text{-}O)>$ = 2.01 Å and $<d(^{IV}Fe^{III}\text{-}O)>$ = 1.86 Å), reduction of Fe-Fe distance from 3.14 to 3.12 Å upon drying is far too small to coincide with a diminished coordination number of surface Fe atoms, whose proportion has been estimated as 35% (Zhao et al. 1993). Reduction of the Fe-Fe distance is instead structurally consistent with the range of Fe-$(H_2O)_I$ distances predicted by our proposed model.

THICKNESS EFFECTS. In transmission mode, the measurement of the absorption coefficient must be performed ideally on thin and perfectly homogeneous sample preparations. Otherwise, so-called "thickness effects" cause a disproportion of the measured amplitude of normalized prepeaks and EXAFS spectra (Stern and Kim 1981). The change in amplitude of the normalized measured signal, S', as compared to the true signal, S, is given by:

$$\frac{S'}{S} = \frac{\Delta\mu_0 x}{1 + \alpha e^{\mu_0 x}}\left[\ln\left(\frac{1 + \alpha}{e^{-\Delta\mu_0 x} + \alpha}\right)\right]^{-1} \quad [4]$$

where x is the sample thickness, μ_0 is the true sample absorption, $\Delta\mu_0$ the true edge step height, and α the percentage of sample pinholes. The parameter α accounts for sample thickness heterogeneity. As illustrated in Figure 1, pre-edge XANES and EXAFS spectra are located opposite each other in relation to the main absorption edge, and thus do not possess the same μ_0 value. Accordingly, the effect of thickness heterogeneity on the normalized signal will be different in both spectroscopies. The change in amplitude for Fe K-EXAFS and pre-edge spectra was calculated for ferrihydrite as a function of the sample thickness x and for several percentages of pinholes (Figure 5). The sensitivity of spectral measurements to sample thickness heterogeneity is quite astonishing. The intensity of prepeak spectra can be easily overestimated by a few tens of percent when samples are thick and inhomogeneous in thickness. The importance of sample thickness to the thickness effect was confirmed experimentally with a thick Fh sample of $\Delta\mu x_{apparent}$ = 2.5 (HFO5), prepared with due precaution by mixing the Fh powder with boron nitride and compacting the mixture. The resulting pre-edge amplitude is enhanced by 30% (Figure 6a) compared to regular samples. Thickness effects, although significantly important, are not believed to fully account for the different Fh prepeak enhancement measurements made by Zhao et al. (1994) (20–80%) and ourselves (0–20%), because a relatively high percentage of pinholes must be inferred, and should be usually noticeable. Zhao et al. (1994) did report that precautions were taken to minimize thickness effects, although the criteria for selection of spectra were unclear. Additional spurious effects need to be envisaged to further explain the discrepancies.

The presence of high X-ray harmonics in the incident X-ray beam also results in a "leakage effect", as harmonics are far less absorbed by the sample than the fundamental beam and do not contribute to the photoelectric process (that is, to the absorption K-edge) (Stern and Kim 1981). This 2nd possible source of prepeak enhancement cannot be excluded as the flux on the X-19A beam line at the National Synchrotron Light Source (NSLS) is higher at 21.3 keV (3rd harmonic) than at 7.1 keV (Fe K-edge), and the sole method of rejecting harmonics was detuning the Si(111) monochromator crystals. This method does not allow complete nullification of the intensity of harmonics (Matsushita and Hashizume 1983).

Thus, there are at least 3 plausible explanations for the origin of the enhanced XANES prepeak intensity for ferrihydrite: 1) inadequate or inapropriate assumptions regarding the oscillator strengths of various Fe sites; 2) structural distortions of surface Fe octahedra due to proximity of H-bonded water and associated changes upon drying; and 3) errors associated with the measurement. Our own measurements agree with a small prepeak enhancement of dry ferrihydrite powders. However, contributions due to experimental uncertainties, such as thickness effects, cannot be totally excluded and may contribute significantly to the increased intensity of dry compared to wet powders. These calculations should alert future experimentalists to the neccessity of taking the greatest care to minimize these possible sources of error.

Main Absorption Edge Spectra

Analysis of the main absorption edge offers additional insights regarding the presence or absence of ^{IV}Fe(III) (Figure 3b). Noteworthy is the resemblance of ferrihydrite spectra to ^{VI}Fe(III) reference spectra and, specifically, the absence of a shoulder ≈5 eV beyond the main edge crest. As discussed in the "Background" section, a marked shoulder is consistently observed in ^{IV}Fe(III)-containing references and is a fundamental feature of tetrahedrally coordinated Fe. Absence of this absorption

https://doi.org/10.1346/CCMN.1997.0450314 Published online by Cambridge University Press

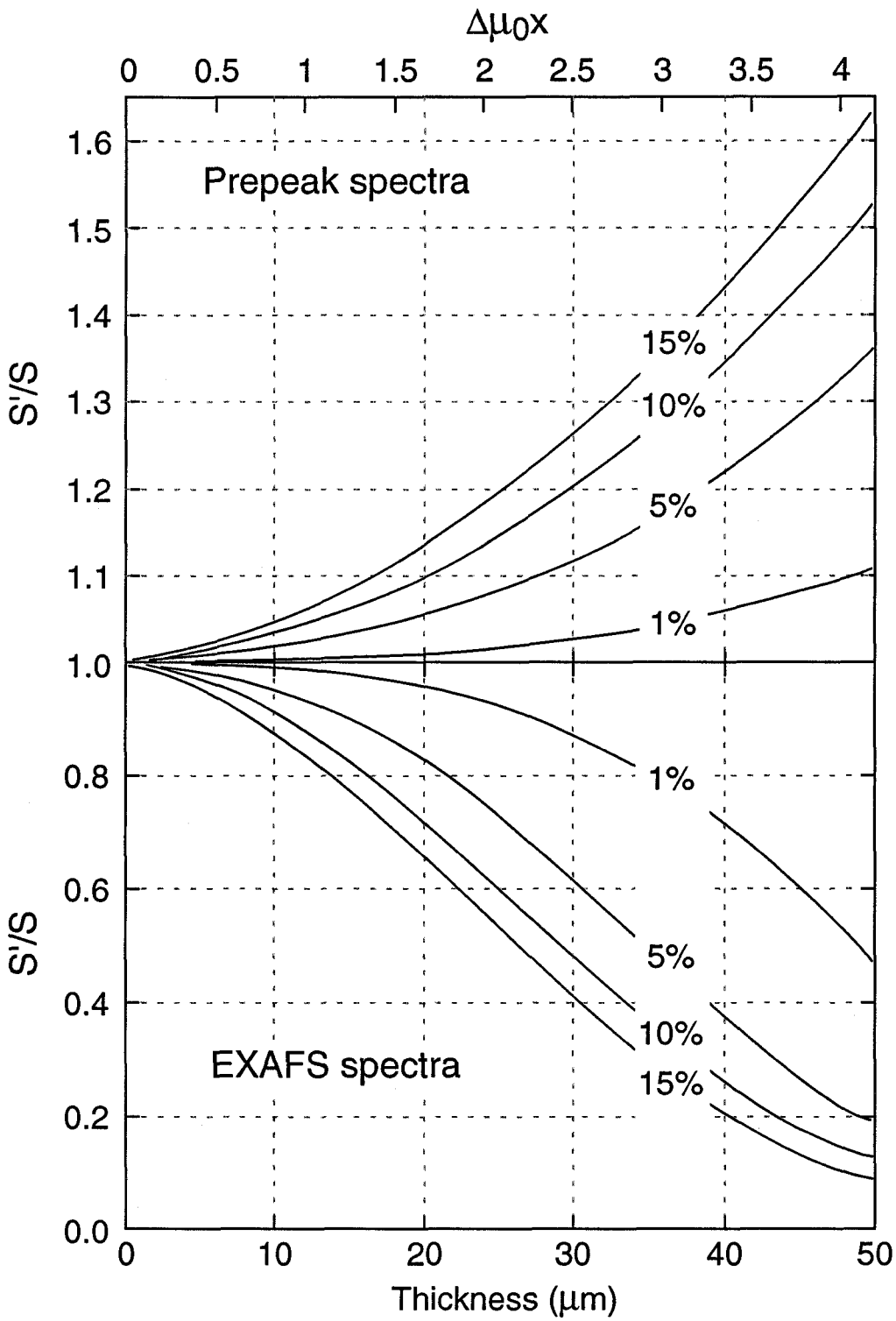

Figure 5. Amplitude of pre-edge and EXAFS spectra for ferrihydrite as function of sample thickness for various percentages of pinholes. Calculations were made by using X-ray absorption cross sections from McMaster et al. (1969).

https://doi.org/10.1346/CCMN.1997.0450314 Published online by Cambridge University Press

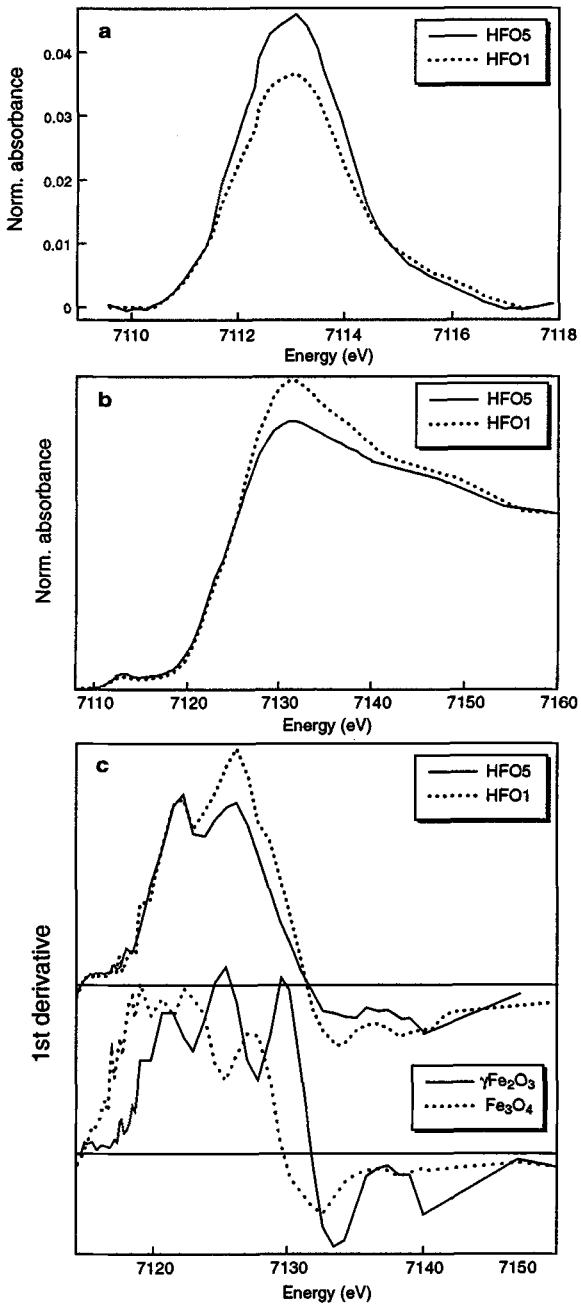

Figure 6. Thickness effects on a) prepeak and b) XANES spectra and c) 1st derivatives of the XANES spectra.

feature in the ferrihydrite spectra indicates the absence of tetrahedrally coordinated Fe.

Comparison of 1st derivative curves improves sensitivity for the determination of ^{IV}Fe(III) species (Figure 7). For tetrahedral coordination, the main-edge shoulder gives rise to notable maxima at 7122 and 7129 eV in the derivative curves (that is, 2 inflection points of the main absorption edge), whereas ferric iron in octahedral

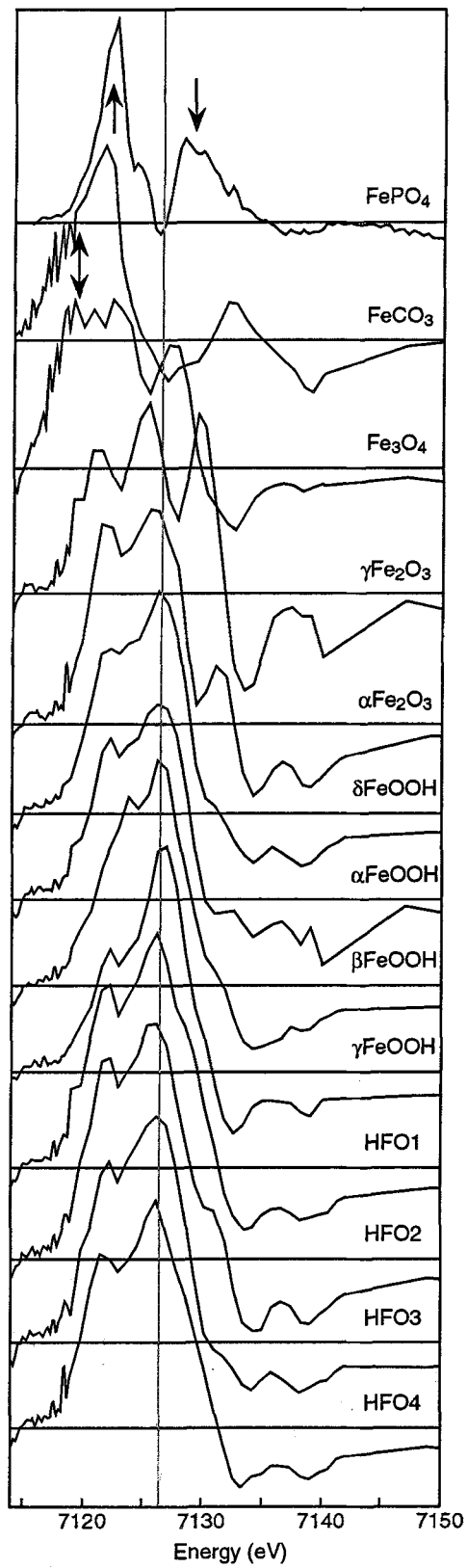

Figure 7. First derivatives of XANES spectra for reference compounds and hydrous ferric oxide samples.

https://doi.org/10.1346/CCMN.1997.0450314 Published online by Cambridge University Press

Table 2. Comparison of EXAFS structural data published in the literature for aqueous Fe colloids and ferrihydrite.

Material		Face-sharing $Fe(O,OH)_6$ octahedra		Edge-sharing $Fe(O,OH)_6$ octahedra	
		R (Å)	*N*	*R* (Å)	*N*
Fe colloids	Partial hydrolysis Fe(III) salt			3.05–3.07	1.8–3.5
Fe colloids	Partial hydrolysis Fe(III) salt			3.02	—
Natural Fh		2.88	—	3.03	—
Natural + synthetic Fh	Full hydrolysis Fe(III) salt				
Synthetic aged Fh	Full hydrolysis Fe(III) salt	2.88–2.89	0.5–1.2	3.05–3.06	3.4–4.1
Synthetic unaged Fh	Full hydrolysis Fe(III) salt			3.05–3.06	3.5–3.7
Synthetic Fh	Full hydrolysis Fe(III) salt			3.00	1.3–1.9
Synthetic Fh	Full hydrolysis Fe(II) salt			3.06	4.5
Synthetic Fh	Heating of iron carbonyl to 500 °C			3.00–3.01	1.2–1.4
Synthetic Fh	Synthetic Fh			2.99–3.01	1.4–2.3

coordination results in a broad maximum centered at 7126 eV. Spectra for multi-site minerals have an intermediate structure, and the presence of $^{VI}Fe(II)$ in Fe_3O_4 is revealed by the broadness of the derivative maximum near 7120 eV. The derivatives for Fh are very similar to the octahedral Fe references, again indicating an absence of tetrahedral Fe in Fh samples.

As shown in the previous section, thickness effects, either originating from sample pinholes or X-ray harmonics, result in a drop of the edge crest intensity and EXAFS amplitude for thick samples (Figures 5 and 6b). However, thickness effects have little influence on the *structure* of main-edge spectra (Figure 6c), and this spectroscopy incidentally appears more reliable than pre-edge spectroscopy for determining the site occupancy of Fe in Fe oxides.

Zhao et al. (1994) concluded from their main-edge analysis that $^{IV}Fe(III)$ was absent, but this finding appeared to conflict with their own interpretation of the prepeak spectra. These contradicting results were accounted for by considering the difference of spatial sensitivity of the 2 techniques. Indeed, pre-edge spectroscopy probes primarily the electronic structure of the excited cation and has low sensitivity to short-range order (that is, beyond the 1st coordination shell). In contrast, resonance features observed on main-edge spectra result from MS pathways of the photoelectron by surrounding atomic shells up to several Å. Accordingly, the lack of evidence for tetrahedral Fe in Fh as deduced from the shape of the main absorption edge was attributed by Zhao et al. (1994) to the absence of extended local order around $^{IV}Fe(III)$ species; specifically, to their location at the grain surface. This interpretation should, however, be discarded in light of recent MS calculations, which showed that spectral features observed a few eV below the edge crest come from single and multiple scattering processes involving only the nearest O shell (Farges 1995). In other words, the shape and intensity of prepeaks *and* of the low-energy part of main absorption edge spectra are determined by both the geometry and electronic properties of the Fe site. To date, results obtained by these 2 independent methods provide little compelling evidence that tetrahedral Fe(III) exists in ferrihydrite.

Comparison with EXAFS Results

The absence of evidence for $^{IV}Fe(III)$ in Fh from XANES spectroscopy is further consistent with all EXAFS studies published in the literature (see references in Table 2). Drits et al. (1993) showed that the detection limit of $^{IV}Fe(III)$ from the quantitative EXAFS analysis of the 1st Fe coordination shell is well below 20–30%. Accordingly, if the ferrihydrite samples studied by Zhao et al. (1994) contained such a high quantity of $^{IV}Fe(III)$, the presence should have been detected by EXAFS.

Zhao et al. (1993, 1994) studied 6 different ferrihydrite samples: 5 were prepared by the hydrolysis of a ferric nitrate solution and 1 by the flame heating of iron carbonyl at 500 °C (30-Å iron oxide catalyst). Two Fe-Fe distances were reported for all these samples: 2.99–3.01 and 3.12–3.15 Å. These values are compared in Table 2 with those determined for similar compounds by different authors. For ferrihydrite samples synthesized from the hydrolysis of a *ferric* iron salt solution, the consensus is that Fe-Fe pairing distances occur at ≈3.0 and 3.4–3.5 Å, characteristic of edge and corner linkage between Fe octahedra. The distance at 3.12–3.15 Å reported by Zhao et al. (1994) for these equivalent samples should be regarded cautiously, as it stands in conflict with all existing EXAFS studies as well as with the proposed ferrihydrite structural model (Drits et al. 1993).

The radial distribution function for the 30-Å catalyst ferrihydrite sample (Figure 6 in Zhao et al. 1993) resembles that published by Combes et al. (1986) for a ferrihydrite sample synthesized by hydrolyzing a *ferrous* salt solution. This 2-line ferrihydrite was characterized as having Fe-Fe pairings at 3.06 Å, lacking a 3.4–3.5 Å Fe-Fe distance, and from comparisons with the structure of well-crystallized Fe oxyhydroxides, was inferred to posses a lepidocrocite-like local structure. This structural result may not be surprising inasmuch as well-crystallized lepidocrocite can easily

Table 2. Extended.

Corner-sharing $Fe(O,OH)_6$ octahedra		
R (Å)	N	Reference
3.43–3.44	1.2–1.5	Combes et al. (1989)
3.45	—	Bottero et al. (1994)
3.44	—	Manceau and Combes (1988) Manceau and Drits (1993)
3.43	1.7–2.0	Combes et al. (1990)
3.43	1.5–1.6	Combes et al. (1990)
3.41–3.45	1.4–2.5	Waychunas et al. (1993)
—	—	Combes et al. (1986)
3.12–3.14	0.6–0.7	Zhao et al. (1993)
3.12–3.15	0.6–1.3	Zhao et al. (1994)

be obtained from the hydrolysis of *ferrous* salts (Schwertmann and Cornell 1991). However, the Zhao et al. (1993) sample differs from that of Combes et al. (1986) by the existence of Fe-Fe pairings at 3.12–3.14 Å. As noted by Zhao et al. (1993), this Fe shell does not fit any Fe shell distance in Fe oxides and thus can unambiguously be assigned to Fe_{bulk}-(O,OH)-$Fe_{surface}$ bonds, since as many as 35% of Fe atoms were estimated to be located near the surface due to the nanometer size of these Fe catalyst particles. Obviously, a modification of the Fe_{bulk}-(O,OH)-$Fe_{surface}$ distance as a consequence of hydration at surface sites should also occur in ferrihydrite particles of larger size obtained by the hydrolysis route (Combes et al. 1989; Combes et al. 1990). However, the fraction of surface Fe atoms in larger hydrolysis products is much lower, making their identification difficult. In addition, in ferrihydrite samples derived from the hydrolysis of *ferric* salt solutions, the detection of Fe-Fe contributions at 3.12–3.14 Å by EXAFS spectroscopy would likely be hampered by the predominant contribution of Fe-Fe pairs at ≈3.01 and 3.4–3.5 Å, corresponding to edge- and corner-sharing octahedra in the bulk sample, respectively (Manceau and Drits 1993).

Based on a polyhedral approach (Manceau and Combes 1988; Manceau and Drits 1993), the Fe-Fe distance of 3.12–3.14 Å can undoubtedly be assigned to an edge-sharing between 2 Fe octahedra, which rules out the assumption of the presence of ferric iron of lower coordination. In solids, metal–metal distances depend primarily on the size and mode of association of coordination polyhedra (Wells 1984). Polyhedral size dependence of Fe(III)-Fe(III) distances can be approximated by considering the ionic radius variation of ferric iron with coordination numbers: $r(^{VI}Fe^{III})$ = 0.645 Å; $r(^{V}Fe^{III})$ = 0.58 Å; $r(^{IV}Fe^{III})$ = 0.49 Å (Shannon 1976). Consequently, an *increase* of the Fe-Fe bulk distance from 3.01 to 3.12–3.14 Å in the particle surface, can hardly be coincident with a *reduction* of coordination number of surface atoms. In our opinion, these simple crystal chemical considerations represent the strongest argument against the interpretation of ferrihydrite XANES and EXAFS spectra by Zhao et al. (1993, 1994).

CONCLUSIONS

A structural model for the surface Fe octahedra of ferrihydrite has been proposed by using the bond–valence theory and polyhedral considerations on the structure of the 2nd solvation sphere. Based on numerous inconsistencies in the quantitative treatment of ferrihydrite XANES and EXAFS spectra, we believe that the estimation of 20–30% tetrahedral Fe in ferrihydrite by Zhao et al. (1993, 1994) is in error. Consideration of H-bond strength differences of sorbed water at surface Fe sites allows a semiquantitative estimation of differences in geometry of the 6-fold surface Fe site between wet and dry samples. Modification of the geometry of the surface Fe site upon drying is believed to account for much of the overestimation of tetrahedral Fe. However, the present study also reveals that the sensitivity of pre-edge spectroscopy to the determination of the site occupancy of Fe in minerals is not very acute, and it is certainly unwise to give too much significance to small variations in the pre-edge intensity. The comparison of Fe oxide reference spectra illustrates the importance of using as many standards as possible in order to check both the self-consistency of the approach and to estimate the uncertainty on the evaluation of the various Fe site populations. Within these constraints, we can anticipate a precision of only 10–15% in the determination of the coordination of various Fe(III) sites in Fe oxides from the analysis of prepeak features in XANES spectra.

ACKNOWLEDGMENTS

The authors would like to acknowledge the French government for covering the cost of living expenses (for W. P. Gates) through a *bourse Chateaubriand.* The LURE staff is also acknowledged for making available the synchrotron facility and the X-ray absorption spectrometer.

REFERENCES

Bajt S, Sutton SR, Delaney JS. 1994. X-ray microprobe analysis of iron oxidation states in silicates and oxides using X-ray absorption near edge structure (XANES). Geochim Cosmochim Acta 58:5209–5214.

Bianconi A. 1988. XANES spectroscopy. In: Koningsberger DC, Prins R, editors. X-ray absorption. Principles, applications, techniques of EXAFS, SEXAFS and XANES. New York: J Wiley, p 573–662.

Bottero JY, Manceau A, Villieras F, Tchoubar D. 1994. Structure and mechanism of nucleation of FeOH (C1) polymers. Langmuir 10:316–319.

Brese NE, O'Keefe M. 1991. Bond-valence parameters for solids. Acta Crystallogr B47:192–197.

Brown ID. 1976. On the geometry of O-H . . . O hydrogen bonds. Acta Crystallogr A32:24–31.

Brown ID. 1981. The bond-valence method: An empirical approach to chemical structure and bonding. In: O'Keefe M, Navrotsky A, editors. Structures and bonding in crystals. New York: Academic Pr. p 1–30.

Brown ID. 1992. Chemical and steric constrains in inorganic solids. Acta Crystallogr B48:553–572.

Brown ID, Altermatt D. 1985. Bond-valence parameters obtained from a systematic analysis of the inorganic crystal structure database. Acta Crystallogr B41:244–247.

Brown ID, Shannon RD. 1973. Empirical bond-strength–bond-length Curves for oxides. Acta Crystallogr A29:266–282.

Calas G, Petiau J. 1983. Coordination of iron in oxide glasses through high-resolution *K*-edge spectra: Information from the pre-edge. Solid State Commun 48:625–629.

Caminiti R, Licheri G, Piccaluga G, Pinna G. 1978. Hydration water–external water interactions around Cr^{3+} ions. J Chem Phys 69:1–4.

Cardile CM. 1988. Tetrahedral Fe^{3+} in ferrihydrite: ^{57}Fe Mössbauer spectroscopic evidence. Clays Clay Miner 36: 537–539.

Chukhrov FV, Zvyagin BB, Gorshkov AI, Yermilova LP, Balashova VV. 1973. Ferrihydrite. Izv Akad Nauk, Ser Geol 4:23–33.

Combes JM, Manceau A, Calas G. 1986. Study of the local structure in poorly-ordered precursors of iron oxi-hydroxides. J Physique C8:697–701.

Combes JM, Manceau A, Calas G. 1990. Formation of ferric oxides from aqueous solutions: A polyhedral approach by X-ray absorption spectroscopy. II. Hematite formation from ferric gels. Geochim Cosmochim Acta 54:1083–1091.

Combes JM, Manceau A, Calas G, Bottero JY. 1989. Formation of ferric oxides from aqueous solutions: A polyhedral approach by X-ray absorption spectroscopy. I. Hydrolysis and formation of ferric gels. Geochim Cosmochim Acta 53:583–594.

Dasgupta DR. 1974. Oriented transformation of chalcophanite during thermal treatment. Z Kristallogr 139:116–128.

Douglas B, McDaniel D, Alexander J. 1994. Concepts and models of inorganic chemistry. New York: J Wiley. 928 p.

Drits VA, Sakharov BA, Salyn AL, Manceau A. 1993. Structural model for ferrihydrite. Clay Miner 28:185–208.

Farges F. 1995. The site of Fe in Fe-bearing $MgSiO_3$ enstatite and perovskite. A theoretical X-ray multiples-cattering study at the Fe *K*-edge. Phys Chem Miner 22:318–322.

Henderson CMB, Cressey G, Redfern SAT. 1995. Geological applications of synchrotron radiation. Radiat Phys Chem 45:459–481.

Manceau A. 1995. The mechanism of anion adsorption on Fe oxides: Evidence for the bonding of arsenate tetrahedra on free $Fe(O,OH)_6$ edges. Geochim Cosmochim Acta 59: 3647–3653.

Manceau A, Charlet L. 1994. The mechanism of selenate adsorption on goethite and hydrous ferric oxide. J Colloid Interface Sci 168:87–93.

Manceau A, Charlet L, Boisset MC, Didier B, Spadini L. 1992. Sorption and speciation of heavy metals on Fe and Mn hydrous oxides. From microscopic to macroscopic. Appl Clay Sci 7:201–223.

Manceau A, Combes JM. 1988. Structure of Mn and Fe oxides and oxyhydroxides: A topological approach by EXAFS. Phys Chem Miner 15:283–295.

Manceau A, Combes JM, Calas G. 1990. New data and a revised model for ferrihydrite: A comment on a paper by R. A. Eggleton and R. W. Fitzpatrick. Clays Clay Miner 38:331–334.

Manceau A, Drits VA. 1993. Local structure of ferrihydrite and feroxyhite by EXAFS spectroscopy. Clay Miner 28: 165–184.

Matsushita T, Hashizume H. 1983. X-ray monochromators. In: Koch EE, editor. Handbook on synchrotron radiation. North Holland. 260 p.

McMaster WH, Kerr Del Grande N, Mallett JH, Hubbell JH. 1969. Compilation of X-ray cross sections. Springfield: US National Technical Information Service.

Muller JE, Jepson O, Wilkins JW. 1982. X-ray absorption spectra: *K*-edges of 3d transitions metals, *L*-edges of 3d and 4d metals, and *M*-edges of palladium. Solid State Commun 42:365–368.

Parfitt RL, Atkinson RJ, Smart RSC. 1975. The mechanism of phosphate fixation by iron oxides. Soil Sci Soc Am J 39:837–841.

Parratt LG. 1959. Electronic band structure of solids by X-ray spectroscopy. Rev Mod Phys 31:616–645.

Pauling L. 1929. The principles determining the structure of complex ionic crystals. J Am Chem Soc 51:1010–1026.

Post JE, Appleman DE. 1988. Chalcophanite, $ZnMn_3O_7$: $3H_2O$: New crystal-structure determination. Am Mineral 73:1401–1404.

Roe AL, Schneider DJ, Mayer RJ, Pyrz JW, Widom J, Que J. 1984. X-ray absorption spectroscopy of iron-tyrosinate proteins. J Am Chem Soc 106:1676–1681.

Russell JD. 1979. Infrared spectroscopy of ferrihydrite: Evidence for the presence of structural hydroxyl groups. Clays Clay Miner 14:109–113.

Schwertmann U, Cornell RM. 1991. Iron oxides in the laboratory. Weinheim: VCH Verlagsgesellschaft mbH. 137 p.

Shannon RD. 1976. Revised effective ionic radius and systematic studies of interatomic ditances in halides and chalcogenides. Acta Crystallogr B25:925–946.

Sherman DM. 1985. The electronic structures of Fe^{3+} coordination sites in iron oxides; Applications to spectra, bonding, and magnetism. Phys Chem Miner 12:161–175.

Spadini L, Manceau A, Schindler PW, Charlet L. 1994. Structure and stability of Cd^{2+} surface complexes on ferric oxides. I. Results from EXAFS spectroscopy. J Colloid Interface Sci 168:73–86.

Stanjek H, Weidler PG. 1992. The effect of dry heating on the chemistry, surface area, and oxalate solubility of synthetic 2-line and 6-line ferrihydrites. Clay Miner 27:397–412.

Stern EA, Kim K. 1981. Thickness effect on the extended X-ray absorption fine structure amplitude. Phys Rev 23: 3781–3787.

Szytula A, Burewicz A, Dimitrijevic Z, Krasnicki S, Rzany H, Todorovic J, Wanic A, Wolski W. 1968. Neutron diffraction studies of α-FeOOH. Phys Status Solidi 26:429–434.

Wadsley AD. 1955. The crystal structure of chalcophanite, $ZnMn_3O_7{\cdot}3H_2O$. Acta Crystallogr 8:1165–172.

Waychunas GA, Brown GE Jr., Apted MJ. 1983. X-ray *K*-edge absorption spectra of Fe minerals and model compounds: Near edge structure. Phys Chem Miner 10:1–9.

Waychunas GA, Brown GE Jr, Ponader CW, Jackson WE. 1988. Evidence from X-ray absorption for network forming Fe^{2+} in molten silicates. Nature 332:251–253.

Waychunas GA, Rea BA, Fuller CC, Davis J. A. 1993. Surface chemistry of ferrihydrite: Part 1. EXAFS studies of the geometry of coprecipitated and adsorbed ansenate. Geochin Cosmochin Acta 57:2251–2269.

Wells AF. 1984. Structural inorganic chemistry. Oxford: Oxford Univ Pr. 1382 p.

Zhao J, Huggins FE, Feng Z, Huffman GP. 1994. Ferrihydrite: Surface structure and its effects on phase transformation. Clays Clay Miner 42:737–746.

Zhao J, Huggins FE, Feng Z, Lu F, Shah N, Huffman GP. 1993. Structure of a nanophase iron oxide catalyst. J Catal 143:499–509.

(Received 20 December 1995; accepted 4 September 1996; Ms. 2721)